Hindawi
Advances in Civil Engineering
Volume 2019, Article ID 9742050, 17 pages
https://doi.org/10.1155/2019/9742050

Research Article

Seismic Performance of Enclosure Wall in Postearthquake Temporary Prefabricated Light-Weight Steel Structure

Guoqi Xing,[1] **Qing-hai Li**,[2] **Jingjie Yu**,[1] **and Wei Xuan**[1]

[1]*College of Civil Engineering and Architecture, Weifang University, Weifang 261061, China*
[2]*China Building Materials Academy, Beijing 100024, China*

Correspondence should be addressed to Guoqi Xing; xgq1105@163.com

Received 27 February 2019; Revised 6 May 2019; Accepted 12 June 2019; Published 24 July 2019

Academic Editor: Melina Bosco

For the postearthquake temporary prefabricated light-weight steel structure, the enclosure walls composed of prefabricated slender columns and prefabricated strip slabs were used in the structure, which were manufactured from construction waste, such as fragments of bricks and tiles, concrete fragments, and chippings of stones. In order to obtain more accurate seismic performance of enclosure walls, a full-scale two-story experimental model was built to be placed on a shake table. In the test, acceleration transducers were fixed to the enclosure walls and steel frame, which were used to obtain the maximum acceleration of the enclosure walls and steel frame as well as natural frequency of the experimental model subjected to the seismic signal including Kobe wave and El-Centro wave. Moreover, pull-on the rope displacement transducers fixed to the exterior walls parallel to the direction of vibration were used to obtain the story drifts. The results of the shake table test show that when the experimental model is subjected to earthquake with maximum acceleration, enclosure walls are not damaged, owing to flexible connection between the steel frame and enclosure walls. Earthquake reduces the stiffness of enclosure walls, and the natural frequency of the experimental model decreases with increasing maximum acceleration of the seismic signal. In addition, based on the acceleration amplification coefficient, the collaborative performance of the steel frame and enclosure wall is better. Besides, when the experimental model is subjected to earthquake with maximum acceleration, the maximum story drift angle is only 1/2615.

1. Introduction

The prefabricated light-weight steel structure in which members were fabricated in factor and assembled onsite had many advantages, such as relatively better construction quality and faster construction speed [1]. Therefore, the structure is often applied to the rural residential. Due to the light weight of the structure, the earthquake resistant behaviour is good and the structure is especially suitable for rural residential [2]. A large amount of construction wastes were produced every year in China. In order to make use of the construction waste, prefabricated slender columns and prefabricated strip slabs were proposed by Xing et al. [3] and applied to enclosure walls (Figure 1) in the postearthquake temporary prefabricated light-weight steel structure. Therefore, the difference between the postearthquake temporary prefabricated light-weight steel structure and conventional light-weight steel structure is the enclosure walls.

For the conventional light-weight steel structure, scholars mainly focus on the seismic performance of beam-to-column joints or end-plate joints and had studied them by the test method. For example, Shi et al. [4] had carried out a series of tests on eight full-scale structural steel beam-to-column end-plate moment connection specimens to study the influence of the parameters on the bearing capacity of the prefabricated light-weight steel structure. Gracia et al. [5] investigated the seismic behaviour of a composite semirigid joint with a double-sided extended end-plate under a series of monotonic and cyclic quasistatic tests. Hu et al. [6] performed a test on full-scale specimens with specific joint configurations under cyclic loading to investigate the seismic performance. Shi et al. [7] proposed an ultralarge capacity end-plate joints with 12 bolts or 16 bolts in tension and four full-scale specimens of ultralarge capacity end-plate joints subjected to monotonic load. Because bolted beam-to-column joints were difficult to be used as connection, Chen and Shi [8] proposed a new

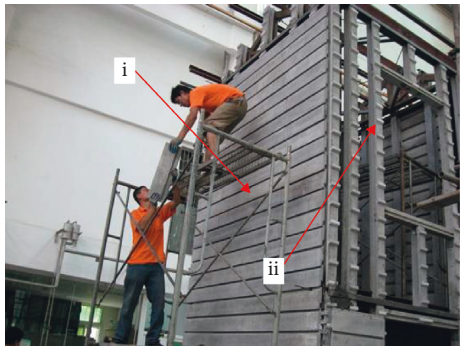

Figure 1: Enclosure wall composed of (i) a prefabricated strip slab and (ii) a prefabricated slender column.

end-plate joint form with box columns and I-section beams, as well as three prefabrication techniques for this connection form, and carried out tests on four full-scale specimens under monotonic loads and cyclic loads. Shi et al. [9] investigated the seismic behaviour of a fully prefabricated steel frame composed of box cold-formed columns, hot-rolled I-section beams, end-plate joints, rod flexible braces, and prefabricated concrete slabs.

In addition, some other scholars had investigated the seismic performance of beam-to-column joints or end-plate joints by the FE method. For example, Shi et al. [10] analyzed the loading resistance and rotational stiffness characteristics of bolted end-plate connections. In order to obtain the rotational behaviour of different three-dimensional configurations as well as the interaction between both major and minor axes, Loureiro et al. [11] investigated a type of three-dimensional joint consisting of extended end-plates for both axes. Shi et al. [12] established a finite element numerical model with the ability to simulate and analyze the mechanical behaviour of different types of beam-column end-plate connections in which all of the bolts were pretensioned. Because the existing design methods of the ordinary or large capacity end-plate joints could not be adopted for ultralarge capacity end-plate joints applied in steel structures involving large spans or heavy loads directly, Chen and Shi [13] proposed a method to predict the moment resistance of the ultralarge capacity end-plate joints.

For the new type of postearthquake temporary prefabricated light-weight steel structure, Xing et al. [3] had already studied the dynamic property. However, the seismic performance of the structure had not been studied. In order to make full use of construction waste and apply the postearthquake temporary prefabricated light-weight steel structure to rural residential, the seismic performance of the structure was investigated by the test method in this paper and the seismic performance of the enclosure walls was studied in particular.

2. Experimental Model and Testing System

2.1. Experimental Model. In order to investigate the seismic performance of prefabricated light-weight steel structure, a full-scale two-story experimental model was built (Figure 2). The detailed dimension of experimental model is shown in Figures 3(a)–3(c). The full-scale two-story experimental model mainly included enclosure walls composed of prefabricated strip slabs and prefabricated slender columns, steel frame composed of steel H beams and steel H columns (Figure 4), precast reinforced concrete floor slab, roof board, etc.

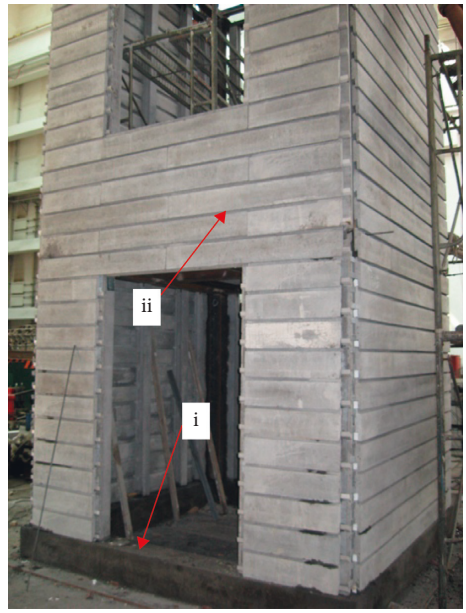

Figure 2: Full-scale two-story experimental model. (i) Ground beam. (ii) Enclosure wall.

For the enclosure walls, prefabricated strip slabs with 180 mm width, 40 mm thickness, and different lengths were placed on the prefabricated slender columns with 100 mm width and 100 mm thickness, which were perpendicular to the prefabricated slender columns as shown in Figure 5. During the construction of the full-scale two-story experimental model, prefabricated slender columns of enclosure wall should be first connected with steel H beams of the steel frame. The bottom of the prefabricated slender column was embedded in the ground beam and the middle of prefabricated slender column, and the top of the prefabricated slender column was connected with steel H beams according to the U-shaped hoop by using bolts, as shown in Figure 6. For the steel frame, the hot-rolled H-shaped steel (HW $125 \times 125 \times 6.5 \times 9.0$ mm) was used as a column and beam. In the experimental model, precast reinforced concrete floor slabs with 60 mm thickness were connected with beams by welding, and fine aggregate concrete with 30 mm thickness was poured to the surface of precast reinforced concrete floor slabs. For the roof board with 60 mm thickness, it was placed on the roof truss. In order to simulate additional gravity load, the weight of 5.76 kN was placed on the surface of floor slab on the second floor (Figure 7(a)) and the weight of 1.73 kN was placed on the roof truss (Figure 7(b)). Total weight of the experimental model was about 117.6 kN. The detailed description for the full-scale two-story experimental model was given by Xing et al. in [3].

2.2. Testing System. In the test, the test system of the shake table simulating earthquake was used, mainly including

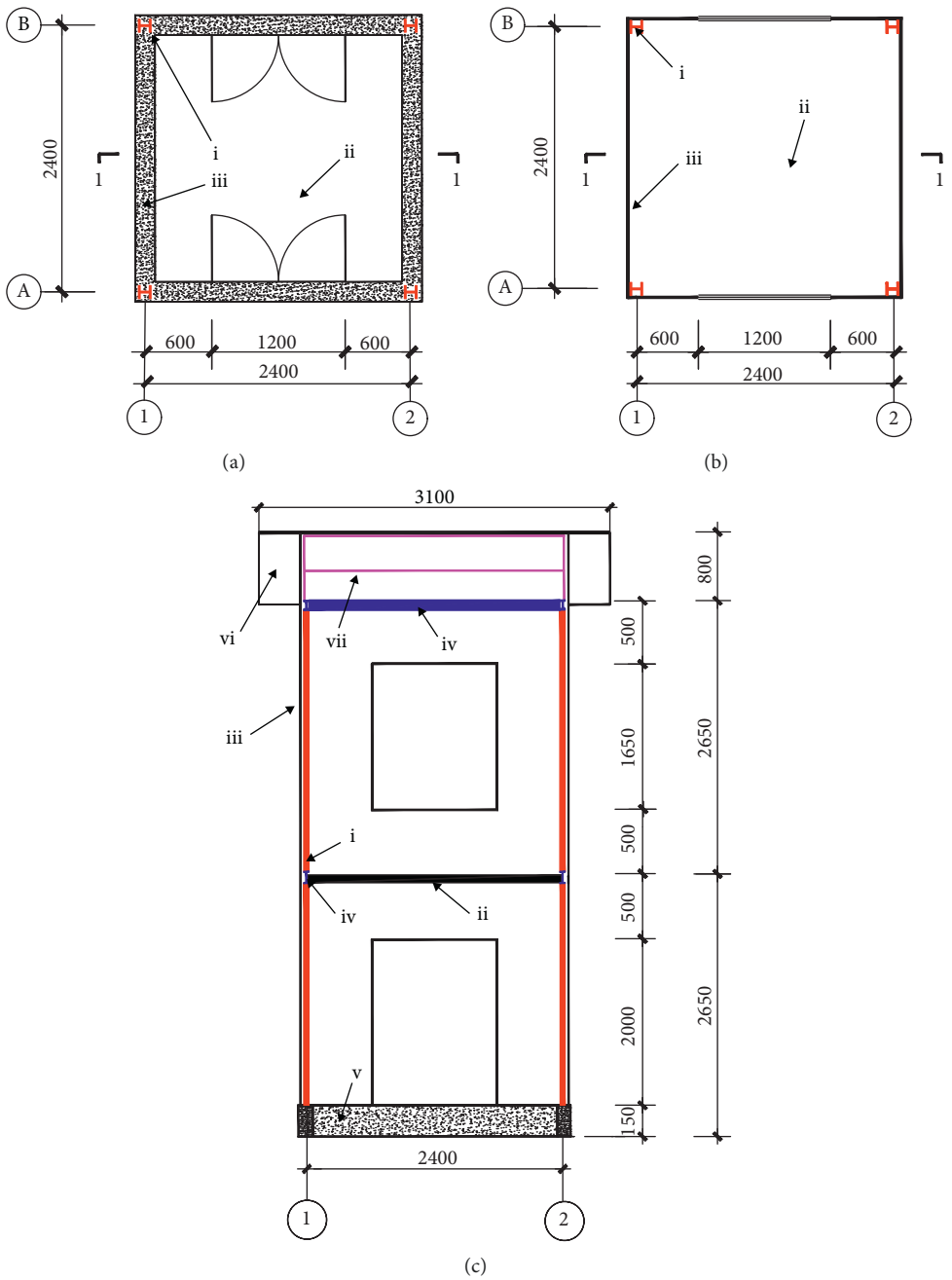

FIGURE 3: Detailed dimension of the experimental model. (a) Plan of the first floor: (i) steel H column, (ii) first floor, and (iii) ground beam. (b) Plan of the second floor: (i) steel H column, (ii) second floor, and (iii) enclosure wall. (c) 1-1 section of the experimental model: (i) steel H column, (ii) precast reinforced concrete floor slab, (iii) enclosure wall, (iv) steel H beam, (v) ground beam, (vi) roof board, and (vii) roof truss. Unit: mm.

shake table, electrohydraulic servo actuator, shake table control system, data acquisition system, etc. as shown in Figure 8. In addition, the parameters for the shake table (Figure 9) used in the test are shown in Table 1.

The test system of the shake table simulating earthquake can be used to study the response and failure mechanisms of the structure subjected to earthquake in the laboratory. In the test system of the shake table simulating earthquake, the shake table can only vibrate horizontally in the test. For the shake table control system, it can be divided into two parts, including simulation control and digital control. Simulation control can generate waveshape with different frequencies; besides, the recorded signal of earthquake with different intensities can also be input into the simulation control. For digital control, it can not only extend or shorten the period of input waveshape but also increase or decrease the maximum acceleration of seismic signal, reducing the distortion of the seismic signal.

During the test, according to the computer control system, seismic signals with different maximum accelerations were

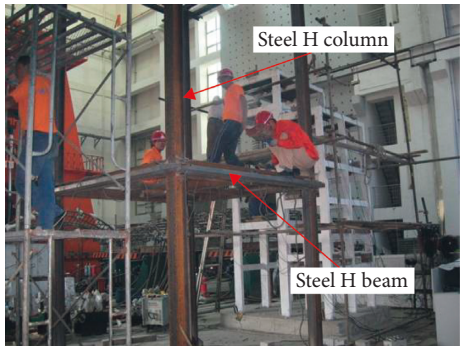

Figure 4: The steel frame composed of steel H beams and steel H columns.

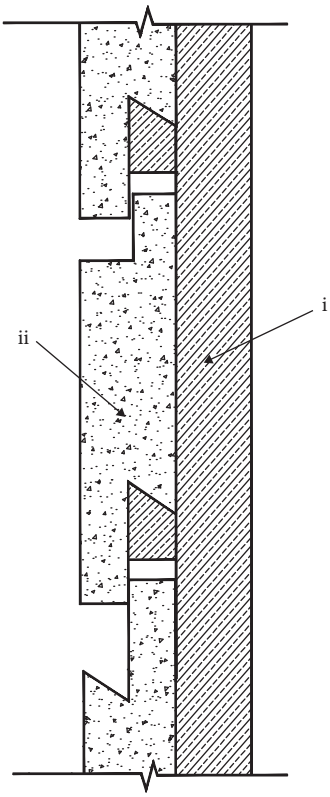

Figure 5: The lateral view of enclosure wall: (i) prefabricated slender column and (ii) prefabricated strip slab.

input into the shake table control system which can control the vibration of the electrohydraulic servo actuator with different maximum accelerations. Then, the electrohydraulic servo actuator can make the shake table vibrate with different maximum accelerations. For the experimental model fixed on the shake table, it can vibrate with the shake table vibrating. During the process of vibration of the experimental model, the signals from acceleration transducers and displacement transducers fixed on different locations of the experimental model can be recorded by the data acquisition system.

In order to investigate the influence of earthquake on the natural frequency of the experimental model, the vibration exciter (Figure 10) was used in the test. For vibration exciters, they can impact the experimental model to make the structure resonate according to inputting the seismic signal into

Figure 6: Flexible connection between the prefabricated slender column and steel H column.

(a)

(b)

Figure 7: Additional gravity load (a) on the floor slab of the second floor and (b) on the roof truss.

vibration exciters. In this paper, vibration exciters were installed on the beams of steel frame in the experimental model. The detailed location for vibration exciters is shown in Figures 11(a) and 11(b). Figures 11(a) and 11(b) show the

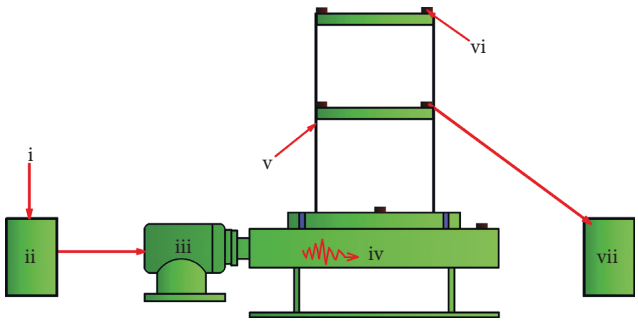

Figure 8: Seismic simulation shake table system. (i) Seismic signal, (ii) shake table control system, (iii) electrohydraulic servo actuator, (iv) shake table, (v) experimental model, (vi) transducer, and (vii) data acquisition system.

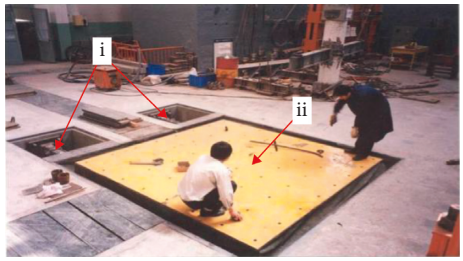

Figure 9: Shake table used in the test. (i) Electrohydraulic servo actuator and (ii) shake table.

plan of top of the first floor and second floor in the experimental model, respectively. In Figure 11(a), vibration exciters notated 1 and 2 were installed on the beam at the top of the first floor. In Figure 11(b), vibration exciters notated 3 and 4 were installed on the beam at the top of second floor.

3. Arrangement of Transducers

3.1. Acceleration Transducer. In the test, the acceleration transducer (Figure 12) installed in the experimental model can be used to obtain the curve of time histories of acceleration and resonance curves. Based on the curve of time histories of acceleration, maximum acceleration of the acceleration transducer can be obtained. In addition, based on the resonance curve obtained from the acceleration transducer, the natural frequency of the experimental model can be determined. In addition, in order to measure the acceleration of the experimental model along the direction of vibration, installation direction for acceleration transducers should be in accordance with the direction of vibration, as shown in Figures 13(a)–13(d).

In Figure 13(a), the acceleration transducer notated 1 was fixed on the middle of the shake table in order to compare the seismic signal obtained from the shake table with that input into the shake table control system. In Figures 13(b)–13(d), in order to obtain the acceleration of the steel frame along the height of the experimental model, acceleration transducers notated 2, 3, and 4 were fixed to the ground beam and the beam on top of the first floor and second floor, respectively. In addition, acceleration transducers notated 3 and 4 also can be used to compare the acceleration of enclosure walls perpendicular to the direction of vibration with that of the steel frame. For acceleration transducers notated 8, 9, and 10, they were used to obtain the acceleration of enclosure walls perpendicular to the direction of vibration along the height of the experimental model, which were fixed to the surface of the enclosure walls, as shown in Figure 13(e). In order to obtain the acceleration of the enclosure walls parallel to the direction of vibration along the height of the experimental model, acceleration transducers notated 11, 12, and 13 were fixed to the surface of the enclosure wall, as shown in Figure 13(f). Besides, in order to compare the acceleration of the steel frame with the enclosure wall parallel to the direction of vibration, acceleration transducers notated 5, 6, and 7 were fixed to the ground beam and the beam on top of first floor and second floor, respectively, as shown in Figures 13(b)–13(d).

3.2. Displacement Transducer. Story drift occurred when the structure was subjected to earthquake, reflecting the deformation capacity of the structure. When the structure was subjected to earthquake, story drift should satisfy the value specified by the Chinese code for seismic design of buildings [14]. In this paper, in order to measure the story drift of the experimental model, pull-on the rope displacement transducer (Figure 14) was used in the test.

In this paper, in order to obtain the story drift of the experimental model, the pull-on the rope displacement transducer was fixed to the surface of the enclosure wall parallel to the direction of vibration. The exact position of the pull-on the rope displacement transducer is shown in Figure 15(a), and Figure 15(b) is the installation diagram for pull-on the rope displacement transducer in site. In Figure 15(a), the pull-on the rope displacement transducers notated 1 and 2 were used to obtain the story drift of the first floor and second floor for the experimental model, respectively.

4. Test Procedure

In order to obtain the seismic performance of the post-earthquake temporary prefabricated light-weight steel structure, two typical recorded seismic signals were used in the test, including the El-Centro wave and Kobe wave. For the El-Centro wave [15], it was widely used in the study of the seismic performance of the structure and the maximum acceleration in the east-west direction and maximum amplitude was 210.1 cm/s^2 and 7.3 m, respectively, as shown in Figures 16(a) and 16(b). For the Kobe wave [15], the maximum acceleration in the east-west direction and maximum amplitude were 818.02 cm/s^2 and 55.1 m, respectively, as shown in Figures 17(a) and 17(b).

In the test, seismic signals with different maximum accelerations were input into the shake table control system which could control the vibration of the electrohydraulic servo actuator, and then the shake table could make the experimental model vibrate. In addition, in the process of the test, maximum acceleration of the seismic signal input into the shake table control system increased with the step of 0.1 cm/s^2 until severe cracks appeared on the surface of the enclosure wall or seismic intensity reached to IX. At the end of the shake table test with different loading steps, the test

Table 1: Parameters for the shake table.

Size (mm)	Dead weight (kN)	Maximum displacement (mm)	Maximum speed (mm/s)	Maximum acceleration (g)	Frequency range (Hz)	Direction of vibration	Vibration wave
3000 × 3000	58.8	±127	±60	±2.5	0.1~50	Horizontal	Seismic signal

Figure 10: Vibration exciter.

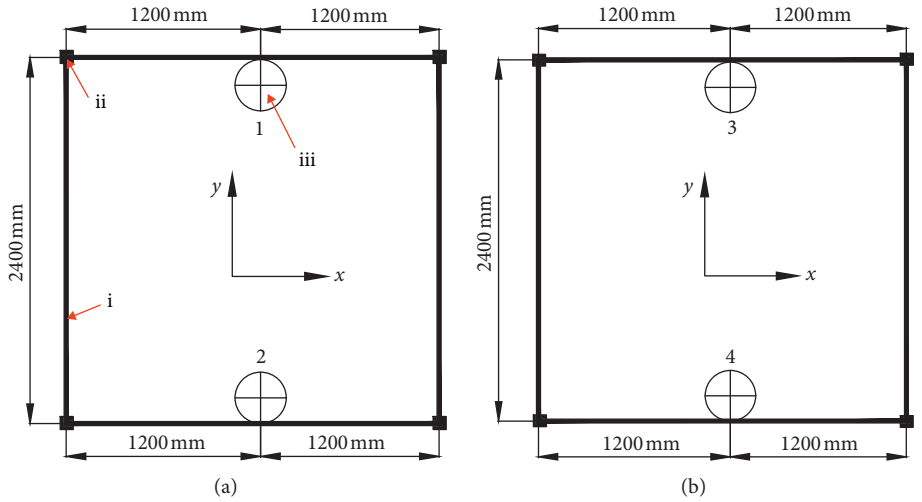

Figure 11: Arrangement of the vibration exciter. (a) Plan of the top of the first floor. (i) Beam, (ii) column, and (iii) vibration exciter. (b) Plan of the top of the second floor.

should be terminated and then we observed whether severe cracks occurred on the surface of enclosure wall or the experimental model was damaged. The detailed procedure for the test is shown in Table 2.

In order to obtain the effect of earthquake on the natural frequency of the experimental model, the resonance test should be carried out before the seismic signal with different maximum accelerations was input into the shake table control system. In the test, the forced-vibration method was used to obtain the natural frequency of the experimental model. When the vibration signal generated by the signal generator was input into the vibration exciter, all vibration exciters would impact the experimental model and the experimental model would resonate when the frequency of the vibration signal was equal to the natural frequency of the experimental model. Based on the acceleration transducers notated 3 and 4 in Figures 13(c) and 13(d), natural frequency of the

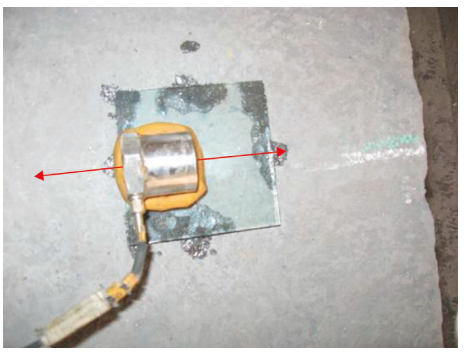

Figure 12: Acceleration transducer. The arrows indicate the installation direction for the acceleration transducer.

experimental model in the Y direction can be obtained. The detailed process for the resonance test is shown in Figure 18. In addition, the method that the natural

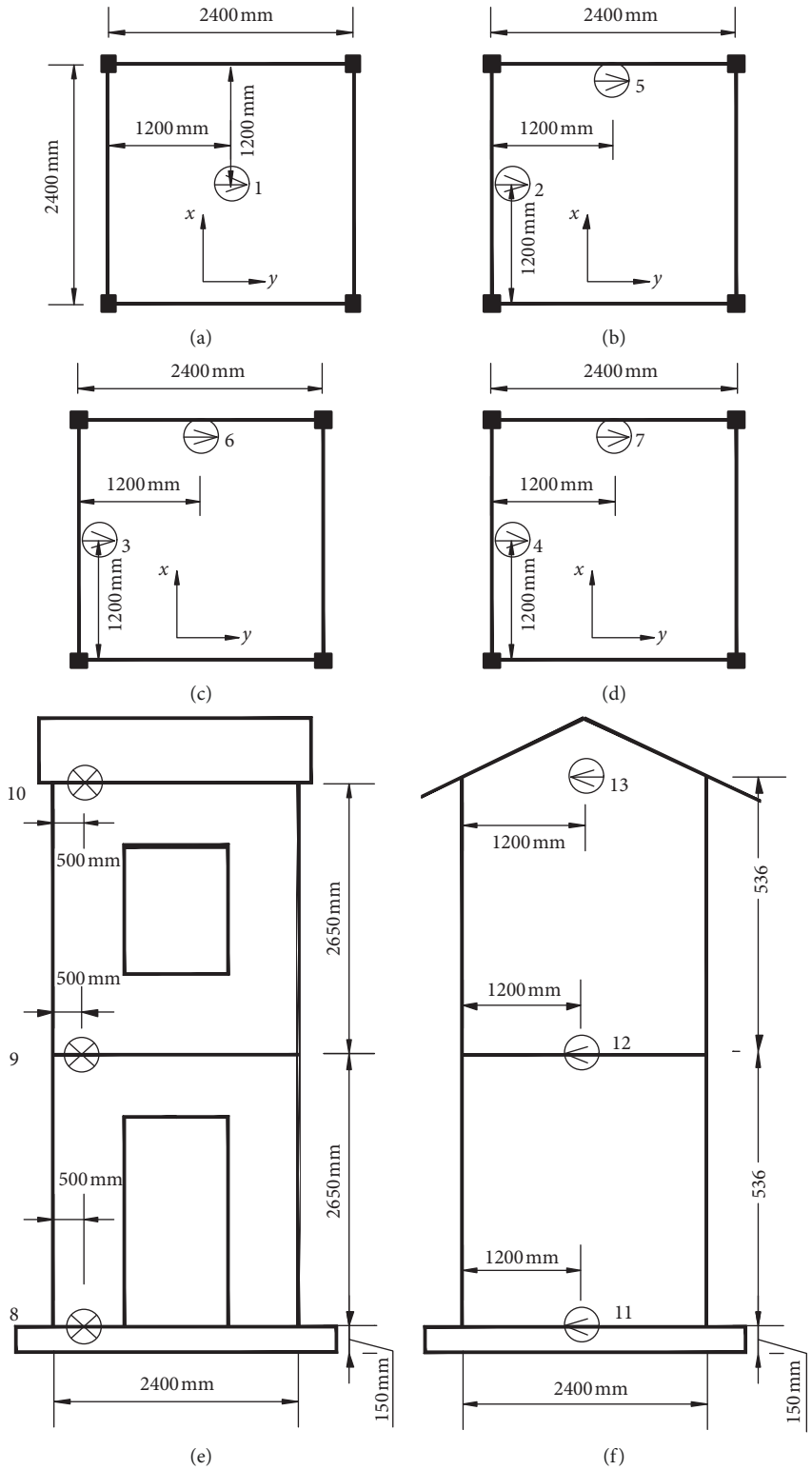

Figure 13: Arrangement of acceleration transducers. Plan of the (a) bottom of the first floor, (b) ground beam, (c) bottom of the second floor, and (d) top of the second floor. (e) Elevation of the wall perpendicular to the direction of vibration. (f) Elevation of the wall parallel to the direction of vibration.

frequency of the experimental model was obtained based on autopower spectra and cross-power spectra of fluctuating signals from acceleration transducers notated 3 and 4 can be referenced from [3].

5. Results and Analysis

5.1. Test Phenomenon. When the Kobe wave with maximum acceleration of 0.4 cm/s^2 was input into the shake table

Figure 14: Pull-on the rope displacement transducer.

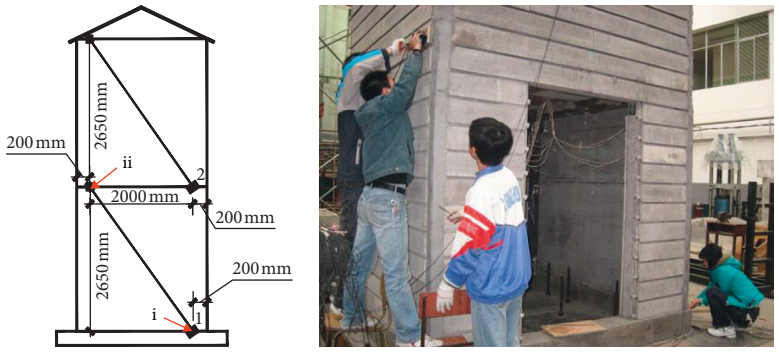

(a) (b)

Figure 15: Arrangement of the pull-on the rope displacement transducer. (a) Elevation of the wall perpendicular to the direction of vibration: (i) pull-on the rope displacement transducer and (ii) end of pull-on the rope. (b) Installation diagram for pull-on the rope displacement transducer in site.

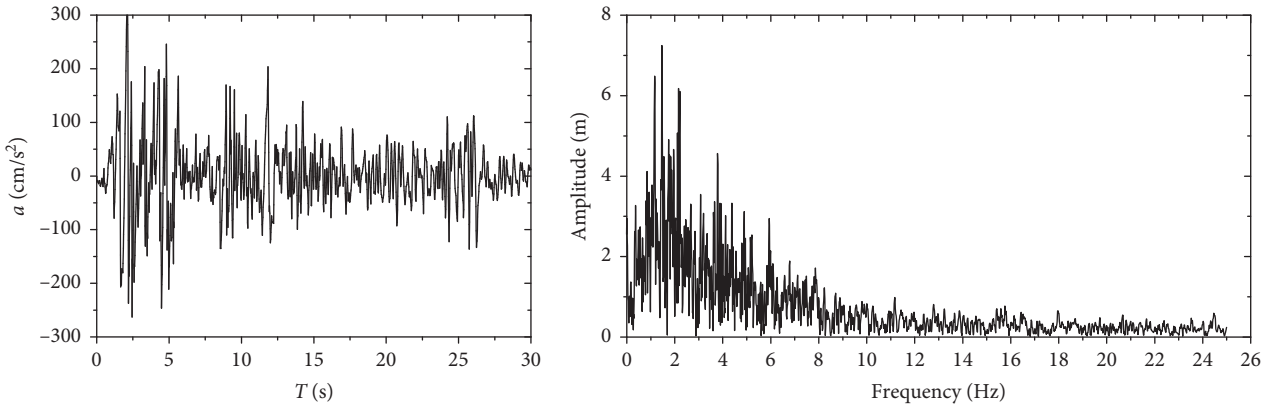

(a) (b)

Figure 16: El-Centro wave. (a) Waveform of El-Centro wave. (b) Spectrum of El-Centro wave.

control system, the experimental model shook very violently, large displacement occurring on top of the experimental model. In addition, the roof board fixed to the roof truss almost fell off the top of the experimental model. Many cracks appeared on the surface of the mortar filled to the corner of the enclosure wall. Besides, cracks also appeared on the surface of prefabricated strip slabs, but prefabricated strip slabs had no fracture. For the flexible connection between the steel frame and enclosure walls, they were not damaged at all.

When the El-Centro wave with maximum acceleration of 0.6 cm/s^2 was input into the shake table control system, shaking of the experimental model was also very violent and a large number of cracks appeared on the surface of mortar filled to the corner of the enclosure wall, but the mortar was not damaged. The roof board fixed to the roof truss fell off the top of the experimental model. In addition, large deformation of the steel frame did not occur and the enclosure walls were also not damaged (Figure 19(a)), a lot of cracks appearing on the surface of enclosure walls. In addition,

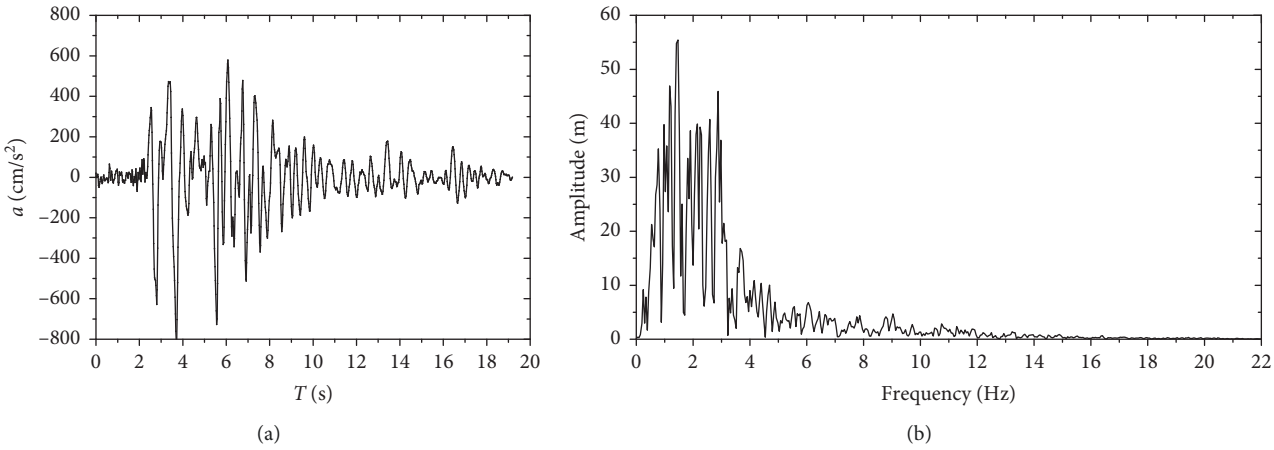

Figure 17: Kobe wave. (a) Waveform of Kobe wave. (b) Spectrum of Kobe wave.

Table 2: Loading procedure for the experimental model.

Serial number	Seismic signal	Maximum acceleration (cm/s^2)	Seismic intensity
Carry out the resonance test and obtain the natural frequency of the experimental model not subjected to the seismic signal			
1	Kobe wave	0.1	V
2	El-Centro wave	0.1	
Observe cracks and carry out the resonance test			
3	Kobe wave	0.2	VII
4	El-Centro wave	0.2	V
Observe cracks and carry out the resonance test			
5	Kobe wave	0.3	VIII
6	El-Centro wave	0.3	VI
Observe cracks and carry out the resonance test			
7	Kobe wave	0.4	IX
8	El-Centro wave	0.4	VII
Observe cracks and carry out the resonance test			
9	El-Centro wave	0.5	VIII
Observe cracks and carry out the resonance test			
10	El-Centro wave	0.6	IX
Observe cracks and carry out the resonance test			

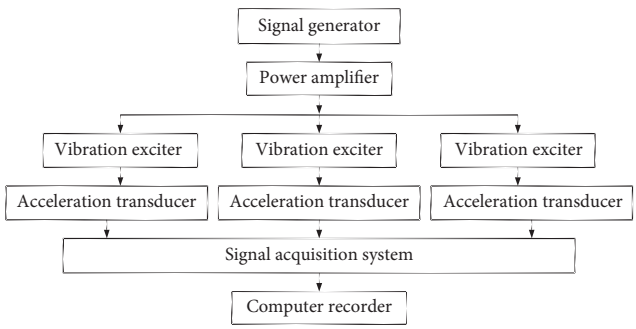

Figure 18: Process of the resonance test.

some flexible connections between the steel frame and enclosure walls parallel to the direction of vibration were slightly damaged. Moreover, the prefabricated strip slabs of enclosure walls parallel to the direction of vibration were loosened relative to the mortar filled to the corner of the enclosure wall, as shown in Figure 19(b). Besides, cracks occurred on the connection of the ground beam and enclosure wall, as shown in Figure 19(c).

5.2. Effect of Earthquake on Natural Frequency. Natural frequency of the structure was related to the stiffness of the structure [16]. Earthquake can reduce the stiffness of the experimental model and has an impact on the natural frequency at the same time. In this paper, we only investigated the influence of the EI Centro wave on the natural frequency of the experimental model. Natural frequencies of the first order and second order of the experimental model subjected to the seismic signal are shown in Figures 20(a) and 20(b), respectively. In Figures 20(a) and 20(b), maximum acceleration of the EI Centro wave equal to 0 indicated that the experimental model was not subjected to earthquake.

As can be seen from Figure 20(a), for the first-order natural frequency of the experimental model, when maximum acceleration of the El-Centro wave was less than 0.4 cm/s^2, earthquake had little effect on the natural frequencies of the experimental model. However, when the maximum acceleration of the El-Centro wave was equal to 0.4 cm/s^2, the natural frequency of the experimental model was much lower than before, due to the stiffness of enclosure walls decreasing and slight damage of the flexible connection

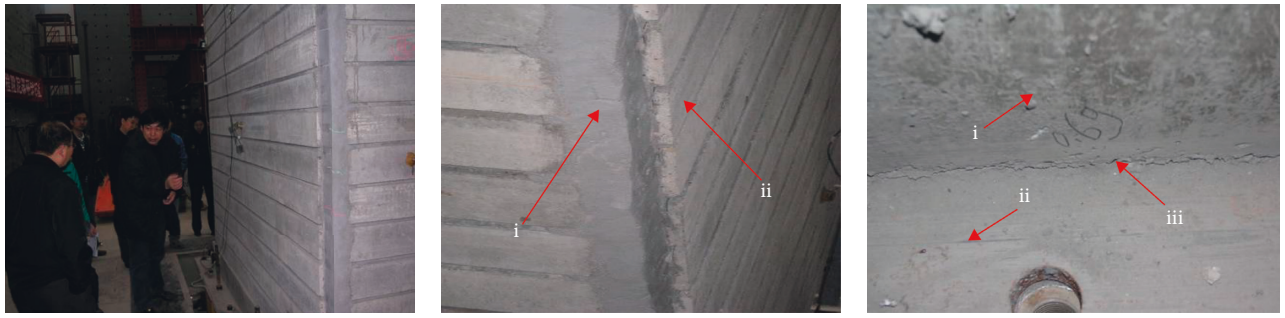

(a) (b) (c)

Figure 19: Test phenomenon. (a) Enclosure walls subjected to earthquake. (b) Loosened prefabricated strip slabs: (i) mortar and (ii) prefabricated strip slab. (c) Cracks on the bottom of enclosure wall: (i) enclosure wall, (ii) ground beam, and (iii) crack.

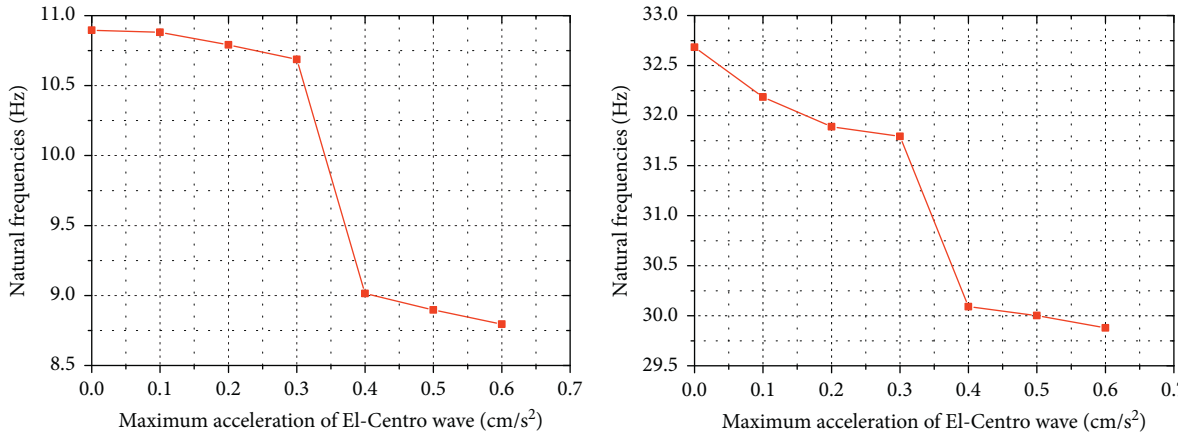

(a) (b)

Figure 20: Natural frequency of the experimental model. (a) First order. (b) Second order.

between the steel frame and enclosure walls. With maximum acceleration of the El-Centro wave increasing, natural frequency continued to decrease. For the second-order natural frequency, the trend was similar to the first-order natural frequency, as shown in Figure 20(b). The results showed that in order to improve the seismic performance of the post-earthquake temporary prefabricated light-weight steel structure, the flexible connection between the steel frame and enclosure wall should be strengthened.

5.3. Maximum Acceleration of Steel Frame and Enclosure Wall. When the experimental model vibrated, the time-history curve in terms of acceleration obtained from acceleration transducers fixed to the experimental model can be obtained, as shown in Figure 21. Based on the time-history curve in terms of acceleration, maximum acceleration of enclosure wall and steel frame can be also obtained.

When Kobe waves with maximum acceleration of 0.1, 0.2, 0.3, and 0.4 cm/s^2 were input into the shake table control system, respectively, the shake table vibrates about one minute and the maximum accelerations of shake table obtained from acceleration transducer noted 1 were 0.1068, 0.227, 0.3639, and 0.486 cm/s^2, respectively. The maximum acceleration of the acceleration transducer fixed to the steel

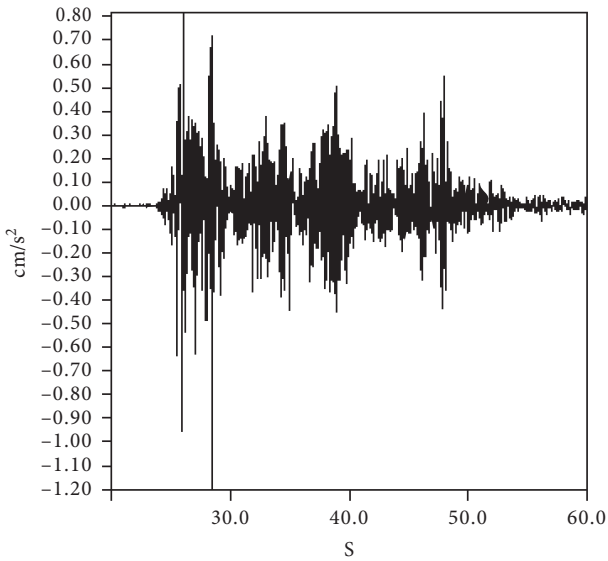

Figure 21: Time-history curve in terms of acceleration.

frame along the height of the experimental model is shown in Figures 22(a) and 22(b), and maximum acceleration of the acceleration transducer fixed to the surface of the enclosure

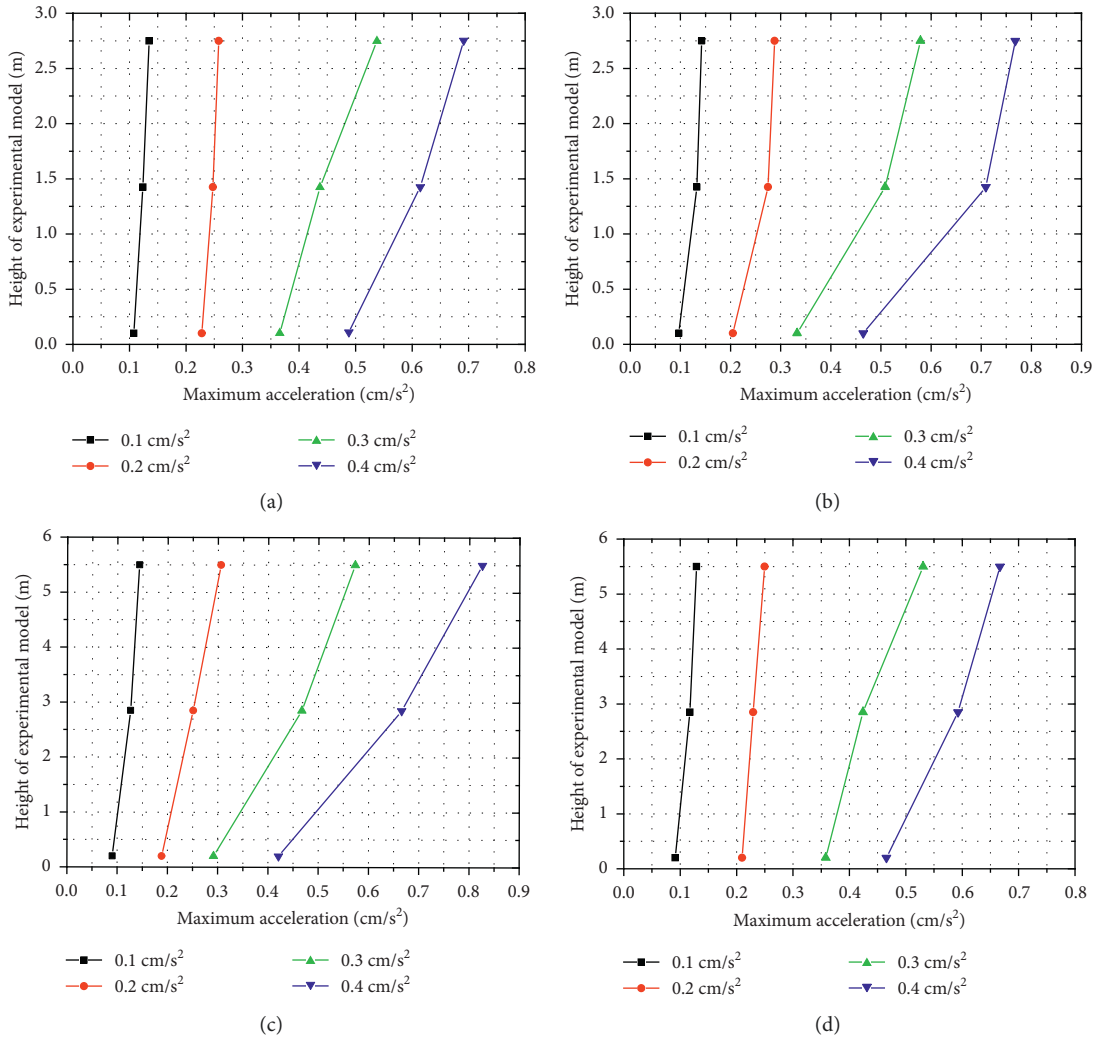

Figure 22: Maximum acceleration under the Kobe wave for the acceleration transducers noted (a) 2, 3, and 4; (b) 5, 6 and 7; (c) 8, 9, and 10; and (d) 11, 12, and 13.

wall along the height of the experimental model is shown in Figures 22(c) and 22(d).

When El-Centro waves with maximum accelerations of 0.1, 0.2, 0.3, 0.4, 0.5, and 0.6 cm/s^2 were input into the shake table control system, respectively, the shake table also vibrates about one minute and maximum accelerations of the shake table obtained from the acceleration transducer noted 1 were 0.1695, 0.2957, 0.4276, 0.5344, 0.6638, and 0.7239 cm/s^2, respectively. The maximum acceleration of the acceleration transducer fixed to the steel frame along the height of the experimental model is shown in Figures 23(a) and 23(b), and maximum acceleration of the acceleration transducer fixed to the surface of the enclosure wall along the height of the experimental model is shown in Figures 23(c) and 23(d).

As can be seen from Figures 22(a)–22(d) and 23(a)–23(d), when seismic signals with different maximum accelerations were input into the shake table control system, maximum acceleration of the acceleration transducer increases with the increase in the height of the experimental model. In addition, maximum acceleration of the acceleration transducer fixed to the surface of the enclosure wall perpendicular to the direction of vibration was larger than that of the enclosure wall parallel to the direction of vibration at the same height of the experimental model. However, at the same height of the experimental model, the maximum acceleration of the acceleration transducers notated 2, 3, and 4 fixed to the steel frame was less than the maximum acceleration of the acceleration transducers notated 5, 6, and 7.

In order to investigate the characters in acceleration for the experimental model, the acceleration amplification coefficient was used in this paper. The acceleration amplification coefficient can be obtained by comparing maximum acceleration of acceleration transducers fixed to enclosure walls and steel frame to maximum acceleration of the acceleration transducer notated 1 (fixed on the shake table). When Kobe waves with maximum accelerations of 0.1, 0.2, 0.3, and 0.4 cm/s^2 were input into the shake table control system, respectively, the acceleration amplification coefficient is shown in Figure 24(a). When El-Centro waves with maximum acceleration of 0.1, 0.2, 0.3, 0.4, 0.5, and 0.6 cm/s^2 were input into the shake table

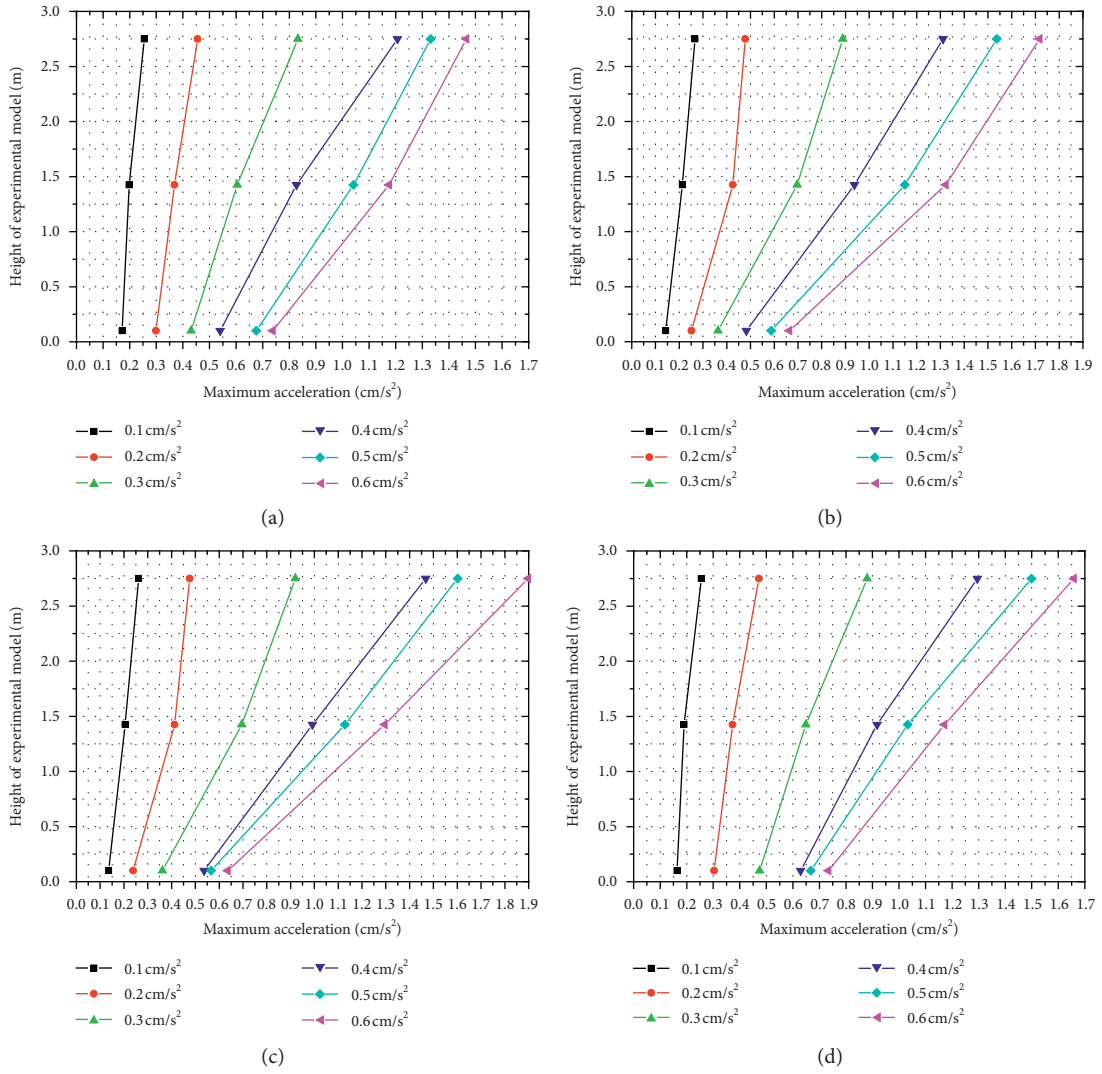

Figure 23: Maximum acceleration under the El-Centro wave for the acceleration transducers noted (a) 2, 3, and 4; (b) 5, 6 and 7; (c) 8, 9, and 10; and (d) 11, 12, and 13.

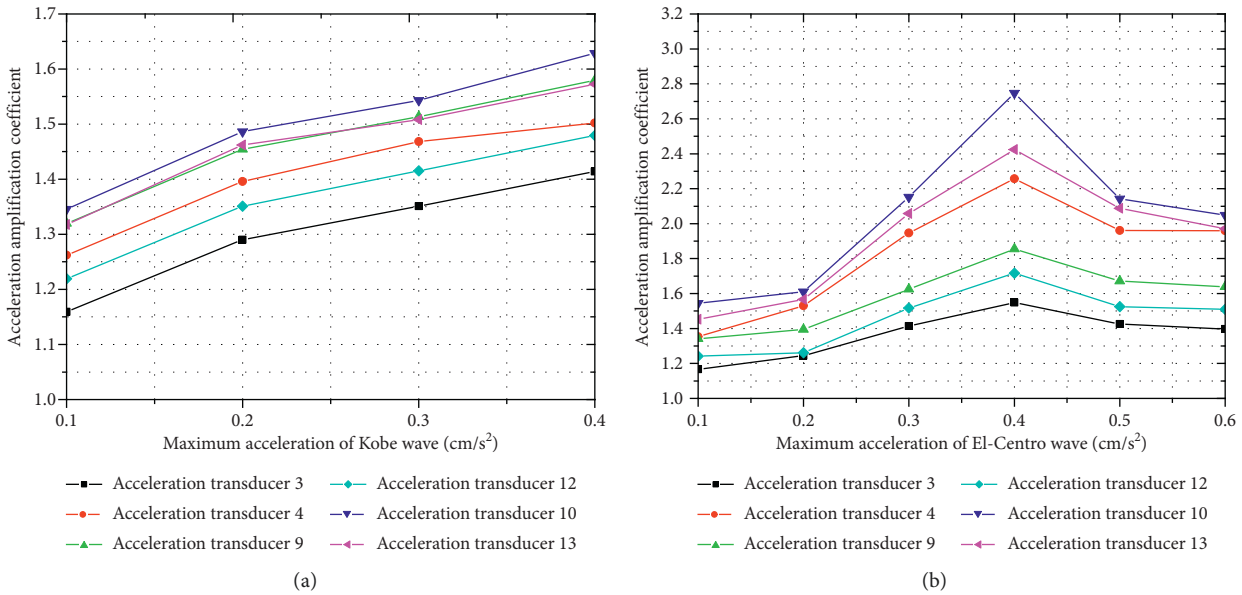

Figure 24: Acceleration amplification coefficient. (a) Kobe wave. (b) El-Centro wave.

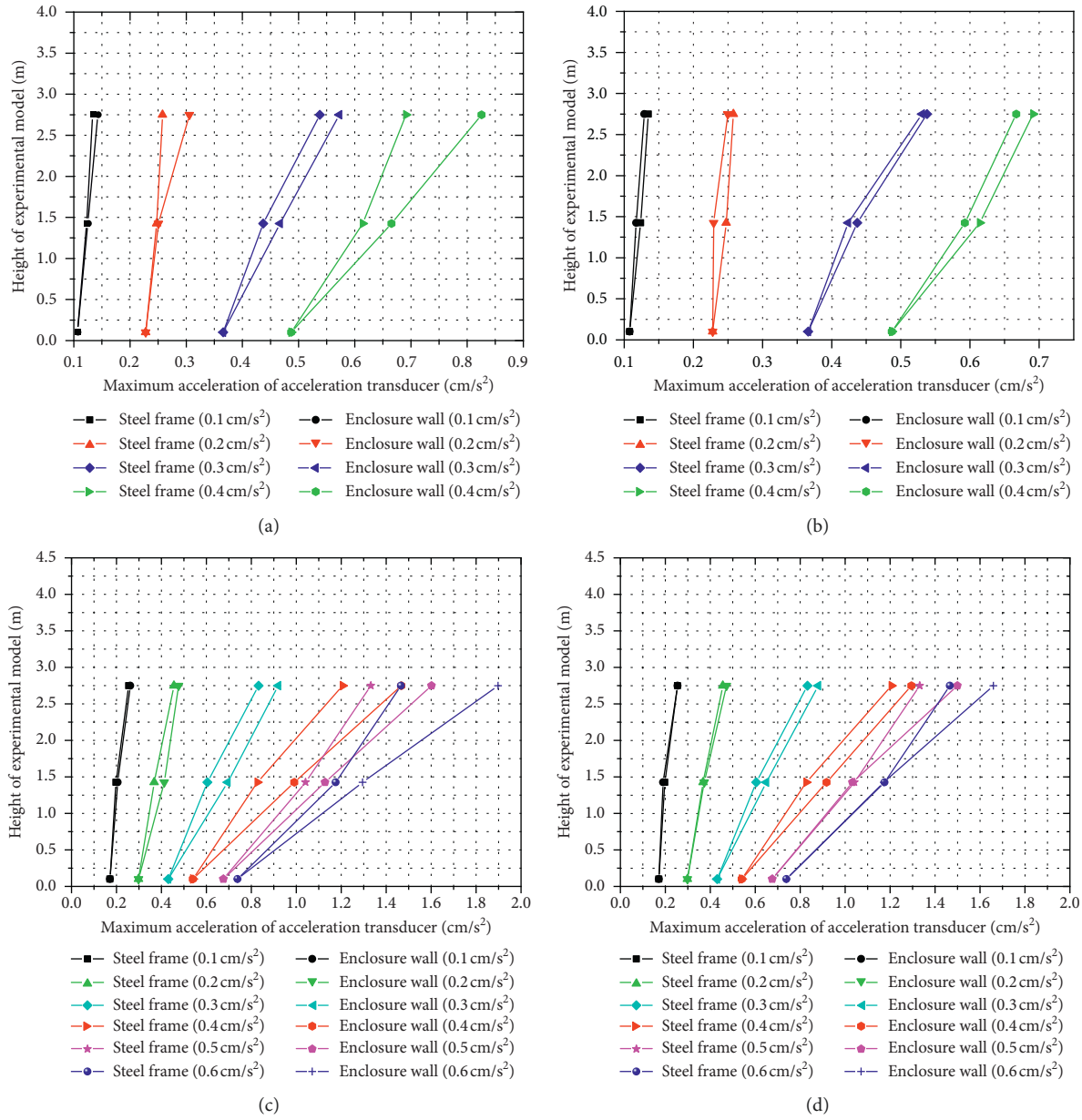

Figure 25: Collaborative performance of the steel frame and enclosure wall. Perpendicular to the direction of vibration under the (a) Kobe wave and (c) El-Centro wave. (b) Parallel to the direction of vibration under the Kobe wave and (d) El-Centro wave.

control system, respectively, the acceleration amplification coefficient is shown in Figure 24(b).

As can be seen from Figure 24(a), with increasing maximum acceleration of the Kobe wave, the acceleration amplification coefficient at different locations is also increased. In addition, at the same height of the experimental model, the acceleration amplification coefficients for enclosure walls were greater than those of the steel frame. Moreover, the acceleration amplification coefficient for the enclosure wall perpendicular to the direction of vibration was greater than that of the enclosure wall parallel to the direction of vibration. As can be seen from Figure 24(b), when maximum acceleration of the El-Centro wave was less than 0.4 cm/s^2, the acceleration amplification coefficient at different locations increased with increasing maximum acceleration of El-Centro wave. However, when maximum acceleration of the El-Centro wave was greater than 0.4 cm/s^2, the acceleration amplification coefficient at different locations decreased slowly with increasing maximum acceleration of the El-Centro wave, due to the degradation of stiffness of the experimental model subjected to earthquake and increased damping.

In order to study the collaborative performance of the steel frame and enclosure wall, we can compare the maximum acceleration of the enclosure wall with the steel frame at the same height of the experimental model. Therefore, based on the results of acceleration of the

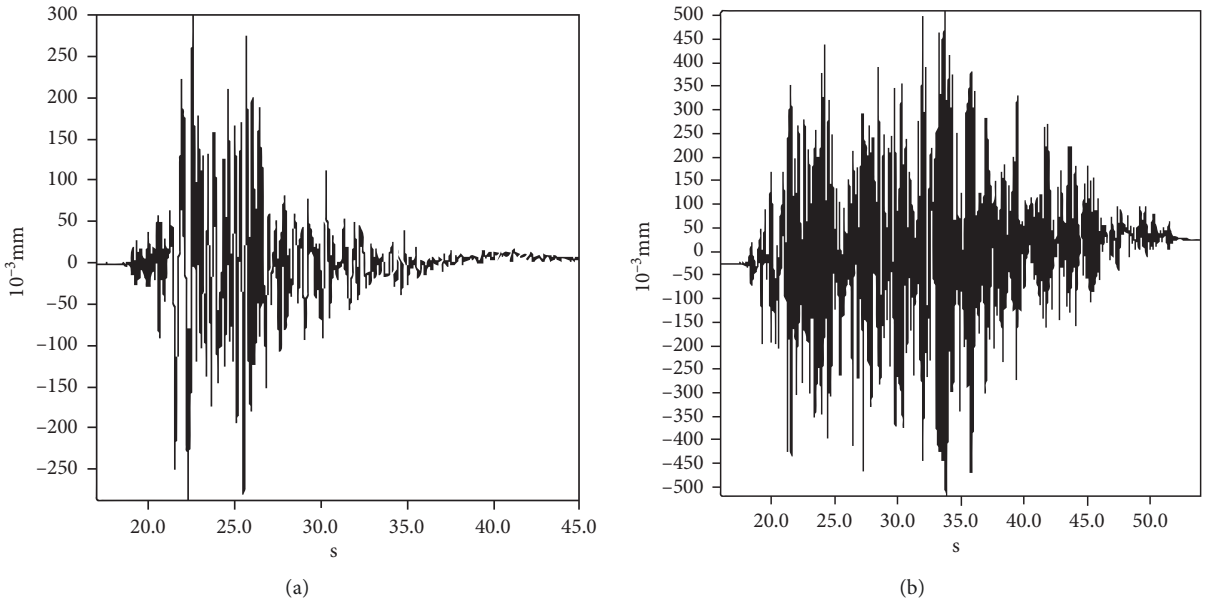

Figure 26: Time-history curve in terms of displacements. Pull-on the rope displacement transducer notated (a) 1 and (b) 2.

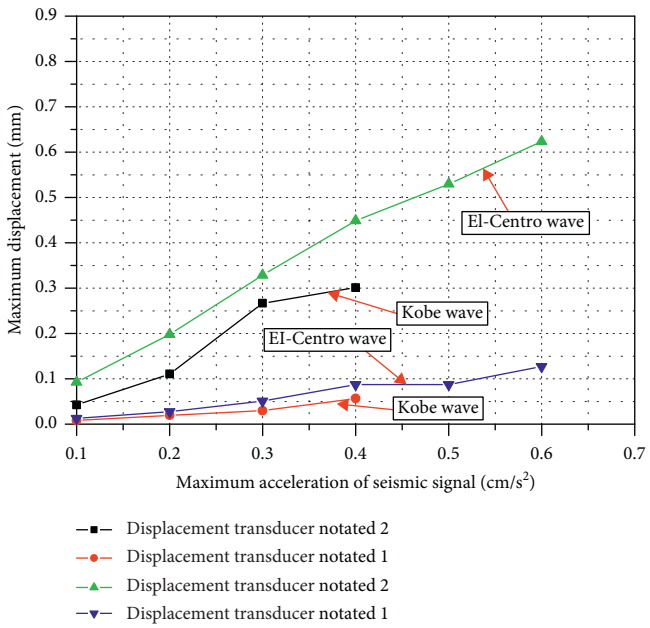

Figure 27: Maximum displacement for the pull-on the rope displacement transducer.

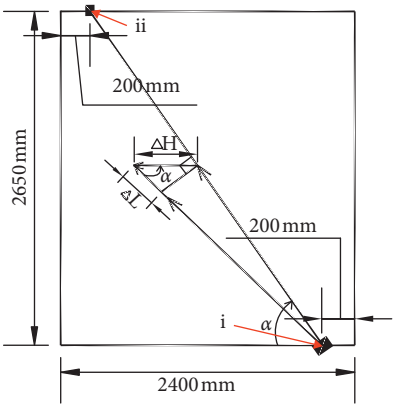

Figure 28: Diagram of relative displacement ΔH along the horizontal direction. (i) Pull-on the rope displacement transducer and (ii) end of pull-on the rope.

enclosure wall and steel frame, comparison of maximum acceleration of the enclosure wall and steel frame at different heights of the experimental model is shown in Figures 25(a)–25(d).

As can be seen from Figures 25(a)–25(d), the collaborative performance of the steel frame and enclosure wall decreased with the increasing height of the experiment model. Comparing with the enclosure wall perpendicular to the direction of vibration, the collaborative performance of the steel frame and enclosure wall parallel to the direction of vibration was better. In addition, when seismic signals with maximum acceleration of 0.1, 0.2, and 0.3 cm/s^2 were input into the shake table control system, respectively, the collaborative performance of the steel frame and enclosure wall was better. However, with maximum acceleration of the seismic signal increasing, a lot of cracks appeared on the surface of the enclosure wall and then the stiffness of the enclosure wall decreased and damping ratio also increased; therefore, the collaborative performance of the steel frame and enclosure walls was worse. In addition, at the same height of the experimental model, the collaborative performance of the steel frame and enclosure walls parallel to the direction of vibration was better than enclosure walls perpendicular to the direction of vibration. In general, due to the application of the flexible connection between the steel frame and enclosure wall, seismic performance of enclosure walls was better.

5.4. Effect of Earthquake on Story Drift. When seismic signals with different maximum accelerations were input into the shake table control system, the shake table would vibrate

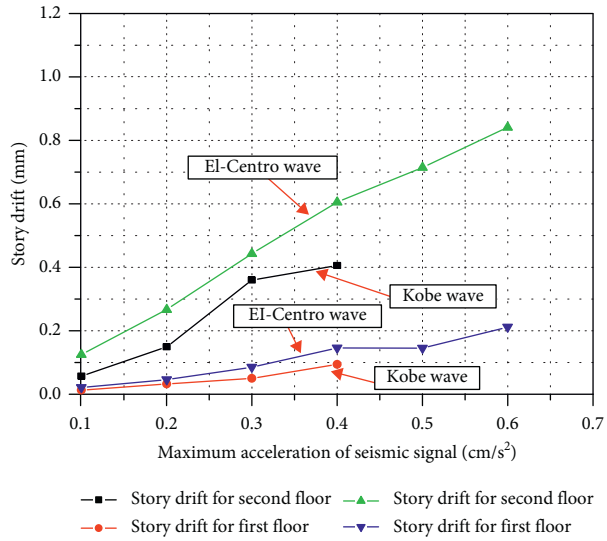

Figure 29: Story drifts under the seismic signal.

Table 3: The drift angle of the experimental model subjected to the seismic signal.

Seismic signal	Storey	Maximum acceleration of the seismic signal (cm/s^2)					
		0.1	0.2	0.3	0.4	0.5	0.6
		Drift angle (rad)					
Kobe wave	First floor	1/166666	1/68111	1/44265	1/23329	—	—
	Second floor	1/38461	1/14725	1/6116	1/5420	—	—
El-Centro wave	First floor	1/103773	1/48034	1/25882	1/15089	1/15120	1/10387
	Second floor	1/17600	1/8245	1/4960	1/3631	1/3078	1/2615

along the horizontal direction, which also made the experimental model vibrate. Based on the pull-on the rope displacement transducers fixed to the enclosure wall parallel to the direction of vibration, the time-history curve in terms of displacements can be obtained. In the test, when maximum acceleration of the Kobe wave was 0.4 cm/s^2, the time-history curves in terms of displacements for the pull-on the rope displacement transducers notated 1 and notated 2 are shown in Figures 26(a) and 26(b), respectively. Based on the time-history curves in terms of displacements, maximum displacement for the pull-on the rope displacement transducer can also be determined. In Figures 26(a) and 26(b), maximum displacement for the pull-on the rope displacement transducers notated 1 and notated 2 was 0.3008 mm and 0.5090 mm, respectively.

When maximum accelerations of the Kobe wave were 0.1, 0.2, 0.3, and 0.4 cm/s^2 and maximum acceleration of the El-Centro wave was 0.1, 0.2, 0.3, 0.4, 0.5, and 0.6 cm/s^2, the maximum displacement for the pull-on the rope displacement transducers notated 1 and notated 2 is shown in Figure 27. As can be seen from Figure 27, the maximum displacement for the pull-on the rope displacement transducer increased with increasing maximum acceleration of the seismic signal. In addition, at the same maximum acceleration of the seismic signal, the maximum displacement for the pull-on the rope displacement transducer notated 2 was larger than that of the pull-on the rope displacement transducer notated 1.

Because the maximum displacement for the pull-on the rope displacement transducers arranged in Figure 15(a) was relative displacement ΔL (shown in Figure 28) along inclined direction, it should be converted to relative displacement ΔH (shown in Figure 28) along horizontal direction according to the following equation:

$$\Delta H = \frac{\Delta L}{\cos \alpha}, \tag{1}$$

where ΔL is the maximum displacement determined by the time-history curve in terms of displacements obtained from the pull-on the rope displacement transducer; α is approximately equal to the angle from the horizontal line to the cable of the displacement transducer, as shown in Figure 28.

Story drift for the first floor and second floor of the experimental model can be obtained based on equation (1), as shown in Figure 29. As can be seen from Figure 29, story drift for the first floor was greater than that of the second floor at the same maximum acceleration of the Kobe wave or El-Centro wave. In addition, story drift increased with increasing the maximum acceleration of the seismic signal.

Based on the relative displacement ΔH along the horizontal direction, the drift angle can be determined as

$$\text{Drift angle} = \frac{\Delta H}{H}, \tag{2}$$

where H represents the story height of the experimental model.

Therefore, based on equation (2) and relative displacement ΔH along the horizontal direction, the drift angle of the first floor and second floor can be determined, as shown in Table 3. As can be seen from Table 3, when the experimental model was subjected to earthquake with maximum acceleration, drift angles were very small and maximum drift angle was only 1/2615 which was much smaller than allowable value of drift angle of earthquake resistant structure 1/300 [14].

6. Conclusions

In this paper, the seismic performance of the post-earthquake temporary prefabricated light-weight steel structure was investigated by the test method. According to the inputting Kobe wave and El-Centro wave into the shake table control system, the full-scale two-story experimental model could vibrate and the following conclusions can be drawn:

(1) The seismic performance of the postearthquake temporary prefabricated light-weight steel structure was good, and the steel frame and enclosure walls composed of prefabricated slender columns and prefabricated strip slabs were not damaged when the experimental model was subjected to earthquake with maximum acceleration. In addition, only a lot of cracks appeared on the surface of enclosure walls.

(2) The natural frequency of the experimental model decreased with increasing maximum acceleration of El-Centro wave, and it dropped sharply when maximum acceleration of the El-Centro wave was equal to $0.4\,cm/s^2$.

(3) Acceleration amplification coefficients for the enclosure wall and steel frame increased with increasing maximum acceleration of the Kobe wave; however, the acceleration amplification coefficients for the enclosure wall and steel frame firstly increased when maximum acceleration of the El-Centro wave was less than $0.4\,cm/s^2$ and they decreased when maximum acceleration of the El-Centro wave was greater than $0.4\,cm/s^2$.

(4) When the maximum acceleration of seismic signals was less than $0.4\,cm/s^2$, the collaborative performance of the steel frame and enclosure wall was good; however, when the maximum acceleration of seismic signals was greater than $0.4\,cm/s^2$, due to the slight damage of the flexible connection between the steel frame and enclosure walls, the collaborative performance of the steel frame and enclosure wall was worse, especially for the enclosure wall perpendicular to the direction of vibration.

(5) Story drifts for the first floor and second floor increased with increasing maximum acceleration of the seismic signal, and story drift for the first floor was greater than that of the second floor at the same maximum acceleration of the seismic signal; when the experimental model was subjected to earthquake with maximum acceleration, the maximum drift angle of the experimental model was only 1/2615 which was much smaller than the allowable value of drift angle of the earthquake resistant structure.

Data Availability

All the data in this paper are obtained from tests in this study, and no other data from the literature are used to support this study.

Conflicts of Interest

The authors declare no potential conflicts of interest with respect to the research, authorship, and/or publication of this article.

Acknowledgments

This work was financially supported by a project of Shandong Province Higher Educational Science and Technology Program (Grant no. J17KB059) and Doctoral Scientific Fund Project of Weifang University (Grant no. 2017BS14).

References

[1] G. Heravi and M. Firoozi, "Production process improvement of buildings' prefabricated steel frames using value stream mapping," *International Journal of Advanced Manufacturing Technology*, vol. 89, no. 9–12, pp. 3307–3321, 2017.

[2] H. M. Xu, Y. Y. Li, and W. Xu, "Dynamic characteristic analysis of prefabricated houses of light-weight steel structure," *Applied Mechanics and Materials*, vol. 578-579, pp. 483–487, 2014.

[3] G. Q. Xing, Q. H. Li, J. J. Yu, and W. Xuan, "Dynamic property of a new type of post-earthquake temporary prefabricated light-weight steel structure," *Advances in Civil Engineering*, vol. 2019, Article ID 7891948, 15 pages, 2019.

[4] G. Shi, Y. Shi, and Y. Wang, "Behaviour of end-plate moment connections under earthquake loading," *Engineering Structures*, vol. 29, no. 5, pp. 703–716, 2007.

[5] J. Gracia, E. Bayo, F. Ferrario, O. Bursi, A. Braconi, and W. Salvatore, "The seismic performance of a semi-rigid composite joint with a double-sided extended end-plate: part I—experimental research," *Engineering Structures*, vol. 32, no. 2, pp. 385–396, 2010.

[6] F. Hu, G. Shi, Y. Bai, and Y. Shi, "Seismic performance of prefabricated steel beam-to-column connections," *Journal of Constructional Steel Research*, vol. 102, no. 11, pp. 204–216, 2014.

[7] G. Shi, X. Chen, and D. Wang, "Experimental study of ultra-large capacity end-plate joints," *Journal of Constructional Steel Research*, vol. 128, pp. 354–361, 2017.

[8] X. Chen and G. Shi, "Experimental study of end-plate joints with box columns," *Journal of Constructional Steel Research*, vol. 143, pp. 307–319, 2018.

[9] G. Shi, H. Yin, F. Hu, and Y. Cui, "Experimental study on seismic behavior of full-scale fully prefabricated steel frame: members and joints," *Engineering Structures*, vol. 169, pp. 162–178, 2018.

[10] G. Shi, Y. Shi, Y. Wang, S. Li, and H. Chen, "Finite element analysis and tests on bolted end-plate connections in steel

portal frames," *Advances in Structural Engineering*, vol. 7, no. 3, pp. 245–256, 2004.

[11] A. Loureiro, A. Moreno, R. Gutiérrez, and J. M. Reinosa, "Experimental and numerical analysis of three-dimensional semi-rigid steel joints under non-proportional loading," *Engineering Structures*, vol. 38, no. 4, pp. 68–77, 2012.

[12] G. Shi, Y. Shi, Y. Wang, and M. A. Bradford, "Numerical simulation of steel pretensioned bolted end-plate connections of different types and details," *Engineering Structures*, vol. 30, no. 10, pp. 2677–2686, 2008.

[13] X. Chen and G. Shi, "Finite element analysis and moment resistance of ultra-large capacity end-plate joints," *Journal of Constructional Steel Research*, vol. 126, pp. 153–162, 2016.

[14] GB50011-2010, *Code for Seismic Design of Buildings*, Ministry of Housing and Urbal-Rural Development of China and General Administration of Quality Supervision, Inspection and Quarantine of China, Beijing, China, 2016.

[15] D. Ivanov, "Origin of earthquakes and seismic waves," in *Seismic Resistant Design and Technology*, pp. 7–66, CRC Press, Taylor & Francis Group, Boca Raton, FL, USA, 2015.

[16] D. F. Gao, J. Liu, F. Li et al., "The researches on shaking table test of Yongning gate embrasure water-tower of Xi'an city wall," *Earthquake Engineering and Engineering Dynamics*, vol. 34, no. 5, pp. 140–149, 2014.